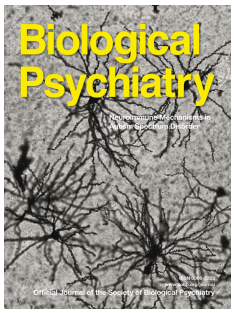

Dimensional and Categorical Solutions to Parsing Depression Heterogeneity in a Large Single-Site Sample

Katharine Dunlop, Ph.D., Logan Grosenick, Ph.D., Jonathan Downar, M.D., Ph.D., Fidel Vila-Rodriguez, M.D., Ph.D., Faith M. Gunning, Ph.D., Zafiris J. Daskalakis, M.D., Ph.D., Daniel M. Blumberger, M.D., Conor Liston, M.D., Ph.D.

PII: S0006-3223(24)00055-6

DOI: https://doi.org/10.1016/j.biopsych.2024.01.012

Reference: BPS 15404

To appear in: *Biological Psychiatry*

Received Date: 7 July 2023

Revised Date: 21 December 2023

Accepted Date: 13 January 2024

Please cite this article as: Dunlop K., Grosenick L., Downar J., Vila-Rodriguez F., Gunning F.M., Daskalakis Z.J., Blumberger D.M. & Liston C., Dimensional and Categorical Solutions to Parsing Depression Heterogeneity in a Large Single-Site Sample, *Biological Psychiatry* (2024), doi: https://doi.org/10.1016/j.biopsych.2024.01.012.

Dimensional and Categorical Solutions to Parsing Depression Heterogeneity in a Large Single-Site Sample

Running Title: Parsing Heterogeneity in Depression

Katharine Dunlop Ph.D.[1,2,3], Logan Grosenick Ph.D.[4], Jonathan Downar M.D., Ph.D.[3,5], Fidel Vila-Rodriguez M.D., Ph.D.[6], Faith M. Gunning Ph.D.[4,7], Zafiris J. Daskalakis M.D., Ph.D.[8], Daniel M. Blumberger M.D.[3,9], Conor Liston* M.D., Ph.D.[4,10]

1. Centre for Depression and Suicide Studies, St. Michael's Hospital, Toronto, Ontario, Canada
2. Keenan Research Centre for Biomedical Science, St. Michael's Hospital, Toronto, Ontario, Canada
3. Department of Psychiatry and Institute of Medical Science, University of Toronto, Toronto, Ontario, Canada
4. Department of Psychiatry, Weill Cornell Medicine, New York, NY, USA
5. Department of Psychiatry & Krembil Research Institute, University Health Network, Toronto, Canada
6. Non-Invasive Neurostimulation Therapies (NINET) Laboratory, Department of Psychiatry, University of British Columbia, Vancouver, British Columbia, Canada
7. Institute of Geriatric Psychiatry, Weill Cornell Medicine, White Plains, NY, USA
8. Department of Psychiatry, University of California San Diego, San Diego, CA, USA
9. Temerty Centre for Therapeutic Brain Intervention and Campbell Family Research Institute, Centre for Addiction and Mental Health, Toronto, Ontario, Canada
10. Feil Family Brain and Mind Research Institute, Weill Cornell Medicine, New York, NY, USA

*Corresponding Author:
413 East 69th Street, Box 240
New York, NY 10021
Telephone: 646-962-6154
Email: col2004@med.cornell.edu

Keywords: Resting-state functional connectivity (RSFC); Major depressive disorder (MDD); Canonical correlation analysis, Functional MRI (fMRI); Biotypes; Subtyping

Abstract

Background: Recent studies have reported significant advances in modeling the biological basis of heterogeneity in major depressive disorder (MDD), but investigators have also identified important technical challenges, including scanner-related artifacts, a propensity for multivariate models to overfit, and a need for larger samples with more extensive clinical phenotyping. The goals of this work were to evaluate dimensional and categorical solutions to parsing heterogeneity in depression that are stable and generalizable in a large, single-site sample.

Methods: We used regularized canonical correlation analysis (RCCA) to identify data-driven brain-behavior dimensions explaining individual differences in depression symptom domains in a large, single-site dataset comprising clinical assessments and resting state fMRI data for N=328 patients with MDD and N=461 healthy controls. We examined the stability of clinical loadings and model performance in held-out data. Finally, hierarchical clustering on these dimensions was used to identify categorical depression subtypes

Results: The optimal RCCA model yielded three robust and generalizable brain-behavior dimensions explaining individual differences in depressed mood and anxiety, anhedonia, and insomnia. Hierarchical clustering identified four depression subtypes, each with distinct clinical symptom profiles, abnormal RSFC patterns, and antidepressant responsiveness to repetitive transcranial magnetic stimulation.

Conclusions: Our results define dimensional and categorical solutions to parsing neurobiological heterogeneity in MDD that are stable, generalizable, and capable of predicting treatment outcomes, each with distinct advantages in different contexts. They also provide additional evidence that RCCA and hierarchical clustering are effective tools for investigating associations between functional connectivity and clinical symptoms.

INTRODUCTION

Major depressive disorder (MDD) is a heterogeneous syndrome assumed to comprise multiple subtypes associated with differing pathophysiological processes, but there is no consensus on how to define them. MDD is diagnosed when a patient presents with five or more of nine criteria, including depressed mood, anhedonia, and changes in sleep or appetite, among others(1–3). Although anxiety is not a core diagnostic criterion, MDD patients often present with comorbid or subclinical anxiety symptoms. Understanding the biological basis of heterogeneity in MDD is a critical challenge for developing new approaches to diagnosis and treatment.

Pioneering work on this topic differentiated clinical MDD subtypes like melancholic, atypical, and seasonal depression based on patterns of co-occurring symptoms or other clinical characteristics (4–7). This approach enabled important advances in our understanding of heterogeneity. However, stable biological substrates of clinical depression subtypes and diagnostic biomarkers remain elusive (4,8–10). An alternative to this approach involves subtyping patients based on shared biological features(11–13), often using neuroimaging-based functional connectivity in depression-related networks(12,14–19). This approach has shown promise in identifying subtypes of psychotic and affective disorders(20–22) and could predict responses to antidepressant medications, psychotherapy, and neurostimulation(23–30).

Recent efforts to parse the neurobiological basis of MDD heterogeneity have taken either a dimensional approach(21,31,32)—using multivariate models to identify continuous brain-behavior relationships—or a categorical approach(17,19,33), clustering subjects into relatively homogeneous categorical subgroups based on shared biological measures. While categorical models may be useful to diagnose disorders and select treatments, dimensional approaches may be more useful for some research purposes, especially where biological measures predict a continuous range of clinical profiles. We(2,34) and others(35,36) have taken a hybrid approach, integrating both models of heterogeneity in depression(31,35) and other neuropsychiatric syndromes like autism spectrum disorder(37) to generate robust, generalizable models of heterogeneity. Previously, we used canonical correlation analysis (CCA(38)) to identify two brain-behavior dimensions defined by co-occurring patterns of resting-state functional connectivity (RSFC) and depressive symptoms: one related to anhedonia and psychomotor slowing, and another associated with anxiety and insomnia(2). Clustering on these dimensions

yielded four MDD subtypes associated with distinct patterns of abnormal RSFC, clinical symptom profiles and responsiveness to repetitive transcranial magnetic stimulation (rTMS). Although two brain-behavior dimensions and a four-cluster solution were optimal, one unanswered question was whether additional dimensions and higher-order clustering solutions could be identified in larger samples.

More recently, investigators have identified important technical challenges to generating multivariate models of heterogeneity using neuroimaging and clinical symptoms. First, our previously reported approach is prone to overfitting(39), and analyses in one report indicate that extraordinarily large sample sizes may be required for detecting reproducible brain-behavior relationships, at least for certain behavioral measures and analytical approaches(40). We subsequently showed that overfitting could be mitigated using regularization and a bootstrapped feature selection procedure(34). Others have shown that with appropriate methodology (e.g., regularization, cross-validation), multivariate analyses can identify replicable effects with substantially smaller sample sizes(41). Second, RSFC data has substantial scanner-related artifacts that may undermine brain-behavior associations; analyses in a larger single-site dataset would eliminate these confounds(34,42,43). Third, more extensive clinical phenotyping may be useful for revealing brain-behavior associations. Our previous work relied on the Hamilton Depression Rating Scale (HRSD) for quantifying depressive symptoms(44). While this scale is widely used for assessing overall depressive severity and has many strengths, it was not designed to comprehensively assess specific symptom domains(45), including anhedonia, a multifaceted hallmark of depression that HRSD represents in a single item(46).

Here, we aimed to develop both dimensional and categorical solutions using updated statistical approaches to parsing heterogeneity in depression in a large, single-site sample, comprising extensive clinical assessments and resting state fMRI data for n=328 patients with MDD. First, we used regularized CCA to identify robust and generalizable brain-behavior dimensions representing the neurobiological basis of individual differences in depression. Next, we used hierarchical clustering on these dimensions to identify categorical MDD subtypes and evaluated their stability and reproducibility. Finally, we characterized both models—dimensional and categorical—by examining associations between specific atypical RSFC features, clinical symptom profiles, and antidepressant responses to rTMS. The optimal RCCA model and clustering solution yielded three brain-behavior dimensions and four depression

subtypes explaining individual differences in clinical symptoms, abnormal RSFC, and rTMS response.

MATERIALS & METHODS

Participants

Participants were recruited at Toronto Western Hospital and the Centre for Addiction and Mental in Toronto, Canada(2,47,48). All participants were enrolled in clinical studies assessing either the antidepressant efficacy of novel cortical targets for rTMS(2,48) or were recruited for a large non-inferiority trial testing the efficacy of novel rTMS protocols over the dorsolateral prefrontal cortex (DLPFC(47)). Inclusion/exclusion criteria and treatment designs are detailed in the supplemental methods; briefly, all participants were 18-65 years old and met DSM-5 criteria. We included participants from our original analysis, since the purpose of this new analysis was to expand upon our methods and evaluate performance under ideal conditions (i.e., using single-site scans). We also included fMRI data from 461 nondepressed participants, 96 of whom were acquired on the same scanner and with identical imaging parameters to the MDD sample. All participants provided written informed consent, and all studies were approved by their site's Research Ethics Board/Institutional Review Board.

Clinical Measures

All participants were assessed at either the screening or baseline by trained assessors on the 17-item Hamilton Depression Rating Scale(44) (HRSD). and either the Beck Depression Inventory I(49) (BDI-II; 65.5%) or the Inventory of Depressive Symptoms (50) (IDS; 34.5%). To gain neurobiological insights on symptoms omitted from the HRSD, we included five composite scores using analogous items from the BDI-II and IDS (supplemental methods): pessimism about the future (IDS#16/BDI-II#2); loss of interest/involvement (IDS#18/BDI-II#12); reduced pleasure/enjoyment (IDS#19/BDI-II#4); difficulty concentrating/decision-making (IDS#14/BDI-II#19 & 13); and irritability (IDS#8/BDI-II#17).

Neuroimaging Acquisition/Preprocessing

All single-site neuroimaging data were acquired on a 3 Tesla GE Signa HDx equipped with an eight-channel phased-array head coil. The neuroimaging acquisition parameters (supplemental methods) have been described elsewhere(51). Resting-state scans were preprocessed using the Analysis of Functional Neuroimages (AFNI) package(52) and is previously reported(2) (supplemental methods). Briefly, we censored volumes and their preceding/following volumes

with a Euclidean Distance >0.3mm; 10.9% of MDD participants were excluded due to high motion. Similarly, 9.4% controls acquired at the same scanner were retained. Whole-brain RSFC was extracted as previously described(2) (**Figure S1**), generating 33,153 features. We evaluated assessed univariate correlations between symptoms and RSFC features were detectable using bootstrapped feature selection. We tested for significance using a permutation test and identified clinical features with greater RSFC features than that expected by chance.

CCA Optimization Overview

To assess canonical variate (CV) generalizability and stability, we first optimized three L2-norm regularized CCA hyperparameters (**Figure S2A**): number of RSFC features, and two regularization terms penalizing the RSFC and clinical matrices, λ1 and λ2, respectively. Each training iteration began by partitioning the data into a two-thirds (*n*=219) training and one-third outer fold (*n*=109; 100 replicates). We further partitioned the outer fold training set into a two-thirds training (*n*=146) and one-third testing inner fold (*n*=73; 20 replicates). Within this inner training dataset, we performed bootstrapped feature selection to identify the most relevant feature. Next, we performed a grid search, modeling different combinations of CCA hyperparameters with the inner training set and assessing the canonical correlation in the inner test set. For each of the 100 outer replicates, the optimal hyperparameter combination was defined as the highest median canonical correlation in test data for CV1. We also assessed the impact of sample size, the strength of correlations, and clinical item range on CCA optimization (supplemental methods/results). Finally, we evaluated the optimal CCA hyperparameters using the outer training set and projected to the outer test partition to generate a final holdout canonical correlation.

Significance Testing

We next sought to characterize dimension generalizability and stability. We defined generalizability as how well each CV performed when applied unseen data, measured as the mean canonical correlation of RSFC and clinical dimension scores. We defined stability as the mean absolute similarity of clinical loadings for each dimension across all training replicates. To test generalizability (**Figure S2B**), we began by partitioning the data into a two-thirds training and one-third test set (1,000 replicates). We performed bootstrapped feature selection using training data to identify the most relevant RSFC features and projected CCA model coefficients to the test dataset to evaluate the canonical correlation. We randomly permuted the testing data (1,000 replicates) to generate a null distribution of canonical correlations. To test

stability (**Figure S3C**), we randomly shuffled participants' clinical data within the two-thirds training set (1,000 replicates). We also calculated the stability of clinical loadings, calculated as the average absolute Pearson's correlation of clinical loadings across all 1000 replicates. For each iteration, we retained CV clinical loadings, generating a null distribution of clinical loading agreement across 1,000 null replicates.

We proceeded to evaluate subsequent CV generalizability using sequential orthogonal deflation, meaning that after we modeled a CV, we orthogonally deflated the data within each iteration to evaluate test canonical correlations for the subsequent CV. We corrected for multiple comparisons accounting for the fact that the canonical correlates are ranked, such that the family-wise error adjusted for the rank-*k* CV corresponded to the cumulative maximum p-value(53). A CV was significantly generalizable or stable at a corrected-$\alpha<0.05$, one-tailed. We proceeded with assessing CVs until neither the generalizability nor the stability was significant.

Characterizing Significant CVs

We next generated a final regularized CCA model for all subjects and significant CVs, using tuned hyperparameters. We evaluated the Bonferroni-corrected clinical loadings and False-Discovery Rate-corrected (FDR) RSFC loadings for each CV.

Hierarchical Clustering

To evaluate clustering performance, we first extracted the Calinski-Harabasz Criterion(54) for 2-10 cluster solutions for combinations of significant CVs. We evaluated criterion values using normalized RSFC CV scores generated from the final model. The optimal cluster solution was identified as the maximum Calinski-Harabasz Criterion value. We used permutation testing (1,000 replicates) to evaluate hierarchical clustering significance. CV scores were generated using randomly permutated clinical and intact RSFC matrices, and Calinski-Harabasz scores were generated for potential solutions. Significant clustering solutions indicated a superior ratio of within to between cluster dispersion (Calinski-Harabasz Criterion) at $p<0.05$, one-tailed.

To test the stability of subtype membership, we generated clusters in two-thirds subsamples of unshuffled data (1,000 replicates). CV scores were generated, and we evaluated the similarity of cluster membership from each subsample replicate to that achieved in the complete sample using adjusted mutual information (AMI). The optimal stability of cluster membership was

defined as the elbow of mean AMI, using the Matlab command "knee_pt." Significance testing was performed using permutation testing (1,000 iterations).

We next proceeded to characterize symptom and RSFC differences by subtype. First, we performed Kruskal-Wallis tests to identify significant differences in symptoms by subtype, and relative to symptom severity of the entire group. Next, we performed Wilcoxon rank sum tests for each RSFC feature and subtype to test for abnormal RSFC relative to controls. We included controls from multiple scanners, including the same site as the MDD sample. To evaluate whether including control data from multiple scanners may have biased our results, we repeated this analysis including only n=96 controls whose data were acquired on the same scanner as the MDD patients and corrected for multiple comparisons whole-brain using the False Discovery Rate. Z-statistics representing atypical subtype-specific RSFC generated using the full and single site control samples were highly correlated (0.978-0.982). We present results obtained from the entire control sample but constrained for features surviving from the analysis using only controls acquired from the same scanner (FDR-p<0.05). We performed a Kruskal Wallis Test for each ROI, using whole-brain Wilcoxon rank sum z-statistics to obtain a test statistic reflecting differences by subtype. The top 25 regions, indicating strong differences in atypical RSFC, were examined in greater detail. Lastly, we identified differences in rTMS response and remission rates using chi-square tests and binomial logistic regression. Statistics were corrected for multiple comparisons (FDR).

RESULTS

Three brain-behavior dimensions explaining heterogeneity in MDD

328/368 participants' scans (215 female, M_{age}=40.4±12.1 [SD] years, range=18-70) were retained following quality control (supplemental methods). Descriptive statistics for demographics and HRSD, BDI-II and IDS scores are summarized in **Tables S1-S3**. Before attempting to build a multivariate model linking brain and behavior, we began by evaluating whether robust correlations between depressive symptoms and RSFC features were detectable in this sample, using bootstrapped feature selection to identify RSFC that were stably correlated with a given clinical symptom score. We tested for significance using a permutation test, and identified clinical features with greater RSFC features than that expected by chance. This analysis identified robust associations between clinical symptoms and RSFC features exceeding what would be expected by chance for 18 of 21 clinical symptoms (**Figure 1A**), with small to moderate effect sizes encompassing thousands of RSFC features.

Next, we used regularized CCA to identify brain-behavior dimensions explaining individual differences in depressive symptoms (**Figure S2A)**. We first identified the optimal regularization parameters that maximized the canonical correlation of the first brain-behavior dimension (canonical variate 1; CV1) in held-out data. The optimal combination (**Figure 1B**) was selected in 98/100 grid search replicates (outer training canonical correlation=0.91±0.01SD; outer test canonical correlation=0.49±0.06SD).

To test the statistical significance of CCA performance in unseen data (**Supplementary Figure S2B**), we generated null test canonical correlations by projecting coefficients modelled using intact training data and shuffled test replicates. The first three brain-behavior dimensions were statistically significant (**Figure 1C**), with canonical correlations in held-out test data ranging from r = 0.23 to 0.47 (Cohen's d = 1.12–1.88, $p < 0.006$). The fourth brain-behavior dimension in this model was not statistically significant in held-out test data (r = 0.08, p = 0.21).

To further validate these results, we also tested the stability of clinical symptom loadings generated during training for each brain-behavior dimension (1,000 replicates, **Supplementary Figure S2C**). To gauge the similarity of clinical symptom loadings across all training replicates, we calculated the absolute correlation between clinical symptom loadings for each dimension, such that higher absolute correlations indicated greater stability in clinical loadings across training replicates. Overall, the clinical symptom loadings were highly stable across training set replicates for the first three brain-behavior dimensions (**Figure 1D**; r = 0.59–0.95, $p < 0.027$ compared to shuffled data). In contrast, the clinical symptom loadings for the fourth brain-behavior dimension were relatively unstable (r = 0.36, p = 0.22 compared to shuffled data). Therefore, all subsequent analyses focused on the first three dimensions identified by regularized CCA.

We next characterized the clinical symptom domains captured in each significant dimension. The first brain-behavior dimension (CV1)—"mood-related connectivity"—explained individual differences in mood, anxiety, fatigue, and somatic symptoms, such that higher dimension scores were associated with greater symptom severity (**Figure 1E**). The second dimension (CV2)—"anhedonia-related connectivity"—explained individual differences in hedonic function and mood symptoms (**Figure 1F)**. Lower CV2 scores indicated greater symptom severity. The third brain-behavior dimension (CV3)—"insomnia-related

connectivity"—explained individual differences in insomnia, especially difficulties with initiating and sustaining sleep (**Figure 1G**), as well as a moderate association with irritability and no association with anhedonia. Individuals with a lower CV3 score had more severe insomnia, while individuals with a higher CV3 score exhibited mild/absent insomnia but more severe irritability. CV3 scores were significantly associated with psychotropic medication use (supplemental results), such that individuals taking serotonin–norepinephrine reuptake inhibitors or non-benzodiazepine sedative hypnotics (e.g. zolpidem) had increased insomnia. CV1 and CV2 scores were not associated with any medication class. Taken together, this analysis revealed three independent brain-behavior dimensions explaining individual differences in distinct depression symptom domains.

To characterize the neurobiological basis of these dimensions, we examined the RSFC feature loadings. To visualize within- and between-network trends, we ranked the top 25 brain regions for each dimension by summed R^2 (**Figure 2A-C**). For CV1, higher scores—indicating higher levels of depressed mood, anxiety, and fatigue—were associated with higher thalamic and basal ganglia RSFC and greater connectivity within the default mode network (DMN; **Figure 2A, Figure S3**). Higher mood-related dimension scores were also correlated with lower RSFC between the DMN, cingulo-opercular network—especially the anterior insula—and frontoparietal control network (e.g., DLPFC; FPN). For CV2, more severe anhedonia (lower score) was associated with higher RSFC within and between the cingulo-opercular control network and the dorsal/ventral attentional networks, and visual network (**Figure 2B, Figure S4**). Canonical reward regions—including the orbitofrontal cortex and anterior cingulate cortex—were also components. Lastly, for CV3, greater insomnia and less irritability (lower CV3 score) were predominately associated with decreased sensorimotor RSFC and RSFC between basal ganglia and the ventromedial prefrontal cortex (**Figure 2C, Figure S5**).

In our previous work in autism spectrum disorder, we found that distinct RSFC features explained heterogeneity in three behavioral domains, but unexpectedly, most features were nonsignificant in case-control comparisons(37). Thus, we tested whether RSFC features explaining brain-behavior heterogeneity were abnormal compared to controls. This analysis showed that most significant RSFC loadings were specific to one brain-behavior dimension (**Figure 2D**; 6,693 features), and only 625 (8.5%) were significantly correlated with ≥2 CVs. A majority (62.7%) of these features fell within the normal range of variation in individuals without depression (**Figure 2E**). Together, these results indicate that individual differences in

depressive symptoms are explained predominantly by variation in specific RSFC features that may be missed when identifying atypical features in a case-control manner.

To better understand the conditions necessary to generate stable and generalizable models of symptom/RSFC heterogeneity, we tested how CCA performance—defined as the first canonical correlation in held-out data—varied as a function of the training sample size and the effect size for univariate correlations between RSFC features and symptoms (supplemental methods). We found that sample size and the strength of univariate correlations impacted both the stability and replicability of the optimal hyperparameter solution (supplemental results; **Table S4**). As expected, increasing the sample size or strength of univariate correlations improved both the stability and performance of this modelling approach.

Hierarchical Clustering Yields Four MDD Subtypes

We used hierarchical clustering to identify relatively homogeneous subgroups of MDD patients in this hybrid brain-behavior space (**Figure 3A-B**). As in our prior work, we began by clustering MDD patients on their component scores for the first two brain-behavior dimensions (canonical variates). To identify the optimal cluster number, we compared the Calinski-Harabasz (CH) criterion value—a measure of cluster quality—for clustering solutions involving 2–10 clusters (**Figure 3C**). To evaluate whether the degree of clustering in each solution exceeded that expected by chance, we generated a null distribution of CH criterion values in shuffled data over 1,000 replicates (**Figure 3D**; see Methods for details). This analysis revealed an optimal clustering solution involving four distinct subgroups of MDD patients (**Figure 3C**) defined by distinct patterns of mood- (CV1) and anhedonia-related functional connectivity (CV2). As in our previous work (2,37), individuals were not distributed into markedly discrete subgroups, but the degree of clustering was significantly greater than chance ($p = 0.004$, **Figure 3D**). For further validation, we assessed the stability of cluster assignments based on hierarchical clustering in bootstrapped subsamples of the data (2/3 of the full dataset across 1,000 replicates), compared to cluster assignments derived from hierarchical clustering on the full dataset. Overall, cluster assignments were stable across subsamples (**Figure 3E**), and the degree of cluster membership concordance for the four-cluster solution was significantly greater than expected by chance ($p < 0.001$, **Figure 3F**). We also tested for higher-order cluster solutions. Hierarchical clustering on all three dimensions did not reveal significant evidence of clustering in this space (**Supplementary Figure S6)**. This does not rule out the possibility of additional clusters, but in this dataset, a four-cluster solution using CV1-2 was

optimal. We also compared our results with clustering on a PCA representation of RSFC features alone (i.e. unconditioned on clinical symptoms). We did not observe statistically significant clustering in any scenario tested (see **Supplementary Results, Supplementary Figure S7** for details). Therefore, all subsequent analyses focused on this solution.

Next, we tested whether the four putative MDD subtypes had distinct clinical symptom profiles. The subtypes did not differ significantly in age (Kruskal-Wallis χ^2=1.026, *df*=3, *p*=0.795, ε^2=0.005), sex (χ^2=4.502, *df*=3, *p*=0.212) or medication status (χ^2 test, FDR-*p*>0.116). However, multiple MDD symptoms varied by subtype (**Figure 3G-I, Tables S5-6**). Subtypes 2 and 3 exhibited the most severe anhedonia, suicidal ideation and anxiety compared to Subtypes 1 and 4. Subtype 1 was associated with low anhedonia and high anxiety and somatic symptoms like appetite loss and fatigue. Subtype 4 had less severe symptoms across a range of domains. As expected, these differences in clinical symptom profiles were associated with subtype-specific connectivity patterns for the mood- and anhedonia-related brain-behavior dimensions but not for the insomnia-related dimension. Specifically, Subtypes 1 and 2 were associated with relatively elevated mood-related connectivity scores (CV1)—predicting higher levels of mood and anxiety symptoms—while Subtypes 1 and 4 were associated with relatively elevated anhedonia-related connectivity scores (CV2)—predicting *lower* levels of anhedonia. Importantly, the purpose of this analysis was to further characterize the MDD subtypes, not to provide an independent validation, since the brain-behavior dimension scores were conditioned on clinical symptoms. (For validation of robustness, generalizability, and predictive power, see RCCA performance in held-out data in Figure 1 and treatment prediction in Figure 4, below.)

Subtyping reveals distinct RSFC abnormalities and rTMS outcomes

We concluded our analyses by evaluating the extent to which the four subtypes defined above were associated with distinct patterns of abnormal RSFC and treatment outcomes. As above, we identified RSFC features that were significantly abnormal in each subtype compared to a reference healthy control dataset comprising 461 individuals (266 females) with no history of depression (by Wilcoxon rank sum test, FDR corrected). To evaluate whether including control data from multiple scanners may have biased our results, we repeated this analysis including only N=96 healthy controls whose data were acquired on the same scanner as the MDD patients. We observed highly similar effects in the analysis restricted to a single scanner (**Supplementary Figure S8**), such that the effects observed in contrasts between MDD patients

and the full sample were highly correlated (r > 0.978) with effects observed in contrasts restricted to a single scanner.

To visualize the neuroanatomical distribution of abnormal connectivity, we identified the 25 ROIs with the most subtype-specific atypical connectivity (**Figure 4A**). These nodes included the bilateral DLPFC, dorsal/ventral higher order visual areas, dorsal striatum, thalamus, and right orbitofrontal cortex. These nodes had divergent network-level trends, with the most anhedonic subtypes exhibiting DLPFC-posterior FPN and DMN-thalamic hyperconnectivity, and subtypes with severe mood and anergia symptoms exhibiting within and between-network hypoconnectivity, except for thalamic hyperconnectivity (**Figure 4B-E**). Subtypes 1 and 4 had the most atypical RSFC (9,214 and 5,692 features, respectively), while subtypes 2 and 3 had the least (3,790 and 2,962 features, respectively. Subtypes with similar dimension scores had more shared atypical RSFC features: for example, subtypes 1 and 2 (associated with greater dimension 1 severity) shared 1,117 abnormal RSFC features. To conclude, subtypes exhibited both common and distinct patterns of atypical RSFC, with the greatest divergence localized to striatal and thalamic regions.

We next determined whether subtype-specific analyses provided more information about atypical RSFC than contrasting all MDD patients with controls (**Figure 4F**). Only 2.4% of features significant in the MDD > control contrast were absent from subtype-specific contrasts (**Figure 4G**). Conversely, 45% of the features significant in >1 subtype were absent, and nearly all (90.5%) abnormal features were specific to one subtype. Lastly, we determined whether subtype-specific atypical RSFC was associated with significant CV loadings. While there was some overlap (**Figure 4H)**, many of the RSFC abnormalities did not significantly explain symptom heterogeneity (39.6%) or *vice versa* (61.7%), indicating that individual differences in depressive symptoms are still explained predominantly by variation in specific RSFC features that falls within the normal range, even after considering subtype-specific abnormalities.

Finally, we tested whether CVs or subtypes predicted rTMS response in MDD patients who received 4-6 weeks of once daily rTMS using intermittent theta burst (TBS) or 10 Hz stimulation over either the DLPFC or DMPFC (*n* treatment completers: DLPFC-10Hz=60, DLPFC-TBS=50, DMPFC-10Hz=49, DMPFC-TBS=45). Antidepressant response and remission to rTMS—irrespective of stimulation site or parameters—was significantly greater

in the two subtypes associated with lower anhedonia (Response: χ^2=4.671, *p*=0.031 Remission: χ^2=5.568, *p*=0.018; **Figure 4I**). We investigated this further using logistic regression predicting remission status. Significant main effects for this model (χ^2=29.722, *df*=10, *p*=0.001, **Table S7**) included the anhedonia dimension CV2 (estimate=1.417±0.570 SE, Odds Ratio(OR)=4.125 [1.350 12.607 95% CI], *z*=2.486, *p*=0.013, **Figure 4J-K**), and sex, such that females were more likely to remit than males (estimate=0.943±0.378 SE, OR=2.569 [1.350 12.607 95% CI], *z*=2.497, *p*=0.013). There was also a significant CV1*Stimulation Parameter interaction, such that 10Hz remitters had lower CV1 scores (less severe mood/somatic symptoms) and *vice versa* for TBS remitters (estimate=1.040±0.509 SE, OR=2.828 [1.043 7.670 95% CI], *z*=2.042, *p*=0.041, **Figure 4L-M**). Cluster membership did not differ with stimulation protocol (χ^2=2.341, *df*=3; *p*=0.505). There were no significant main or interaction effects by stimulation site (*p*>0.652). Consistent with our previous finding(2), the results indicate that favorable rTMS outcomes are associated with less severe anhedonia.

DISCUSSION

In an extension of previous work, we characterized regularized CCA and clustering performance in a large, single-site MDD dataset. Both regularized CCA and hierarchical clustering demonstrated significant performance and stability. The final CCA model yielded three dimensions: mood/somatic symptoms linked to thalamic/DMN RSFC; anhedonia correlated with visual and cingulo-opercular RSFC; and insomnia associated with sensorimotor and posterior insula RSFC. Dimension scores grouped participants into four homogeneous subtypes, each with distinct symptom severity, abnormal RSFC, and rTMS responsivity.

We also identified situations with potential limitations: *n*<150 or univariate brain-behavior correlations $\rho \leq .10$ resulted in poor model performance and stability. Other unassessed situations, such as item range or distribution in subclinical populations, may be problematic for this approach. fMRI quality could also negatively impact the strength of correlations, and ideally scans should be of long duration. Multi-echo fMRI may also help to resolve issues of data collection duration and quality(55), however such data has yet to be used in such an analysis.

CCA revealed three dimensions resembling well-documented MDD symptom-brain associations. CV1 correlated mood-related symptoms with increased DMN RSFC and decreased DMN-cingulo-opercular RSFC, consistent with negative self-referential processing

in MDD(16,56,57), sad mood induction(58) and elevated peripheral inflammatory marker(59). Elevated thalamocortical RSFC characteristic of this dimension is implicated in depressive symptomatology in animal models(60) and melancholic depression(61). CV2, associated with anhedonia, correlated with attentional and cingulo-opercular RSFC implicated in reward processing and effort valuation(31,60–62). However, this dimension was not associated with canonical reward processing regions, such as the ventral striatum. Anhedonia symptoms were also modestly but significantly associated with CV1, where the top RSFC features included reward processing regions like the striatum and DMN, so some of the striatum-related variance may have been captured by CV1. CV3, associated with sensorimotor and posterior insula RSFC, implicated regions linked to aberrant homeostatic regulation in insomnia(63–65)(66).

MDD subtypes differed in symptom severity and atypical RSFC, which differ slightly from our previous publication(2). Given the difference in the analyses, including a nested grid search, bootstrapped feature selection and regularization, we would not necessarily expect the same results. We previously reported on subtypes delineated on anhedonia and anxiety/insomnia dimensions, and like that the first two dimensions in our updated analysis represent mood/anxiety and anhedonia. However, insomnia symptoms separated into a third, distinct dimension, which was omitted during clustering as its inclusion did not yield significantly homogeneous clusters.

Despite updates in our approach, similarities in subtype-specific atypical RSFC were observed(2), like subcortical hyperconnectivity in anhedonic subtypes and subtypes with severe fatigue showed orbitofrontal hypoconnectivity. Lower anhedonic symptoms were most responsive to DMPFC or DLPFC rTMS, consistent with our previous study (2). Previous rTMS studies implicate baseline anhedonia in excitatory rTMS response over the DMPFC(51) or DLPFC(28,69,70). A clinical trial is underway to assign rTMS treatments based on subtype assignments (NCT04041479), which is needed to validate the prospective clinical utility of this approach. An analogous approach could be extended to other antidepressant interventions to identify a system for subtyping individuals that would predict response to multiple types of interventions.

We note several caveats. First, this study is not a replication of our previous findings as we included some participants from the original analysis(2); rather it represents an analytic extension with nearly threefold more participants scanned at the same site. Nevertheless, the

current results support future MDD subtyping endeavors and replication attempts using RSFC. Second, the CV and subtypes could be sensitive to dataset idiosyncrasies like study design or clinical assessments; for example, both age(71) and sex(72) impact normative and depressed RSFC. Participants included in the current study were referred for rTMS, meaning they were treatment-resistant, taking psychotropic medications, and predominately moderate-to-severely depressed. Although our original and current analysis indicate that subtype assignment does not differ by medication status(2), RSFC changes due to psychotropic medication have been previously reported(73–79), including in non-remitters(80) and after discontinuing medication(81). Third, the results are likely influenced by our choice of clinical inputs. Future studies would benefit from less coarse assessments of depressive severity, perhaps by quantifying domain-specific impairments, like the Pittsburgh Sleep Questionnaire for insomnia/hypersomnia(82). Future studies should consider refining assessments and validating clinical differences using independent measures.

To conclude, this study evaluated neurobiologically-based MDD subtyping methods, demonstrating superior performance and stability. A four-cluster solution was optimal, and subtype membership correlated with rTMS response. These results represent an important step forward in assessing data-driven subtyping methods and provide evidence supporting the utility of regularized CCA in identifying stable and generalizable associations between RSFC and behavior.

Disclosures

KD was supported by a CIHR Banting Postdoctoral Fellowship and is currently supported by a University of Toronto Department of Psychiatry Academic Scholars Award. CL is supported by grants from the National Institute of Mental Health, the National Institute on Drug Abuse, the Rita Allen Foundation, the Klingenstein-Simons Foundation, the Brain and Behavior Research Foundation, the Hope for Depression Research Foundation, and the Pritzker Neuropsychiatric Disorders Research Consortium.

KD is listed as an inventor on Cornell University patent applications on neuroimaging biomarkers for depression that are pending or in preparation. JD reports research grants from CIHR, the National Institute for Mental Health, Brain Canada, the Canadian Biomarker Integration Network in Depression, the Ontario Brain Institute, the Klarman Family Foundation, the Arrell Family Foundation, and the Edgestone Foundation; reports travel stipends from Lundbeck and ANT Neuro, reports in-kind equipment support for investigator-initiated trials from MagVenture, and is an advisor for BrainCheck, NeuroStim TMS and Salience Neuro Health. FVR receives research support from CIHR, Brain Canada, Michael Smith Foundation for Health Research, Vancouver Coastal Health Research Institute, and Weston Brain Institute for investigator-initiated research; philanthropic support from Seedlings Foundation; in-kind equipment support for this investigator-initiated trial from MagVenture; and honoraria for participation in advisory board for Janssen. ZJD has received research and equipment in-kind support for an investigator-initiated study through Brainsway Inc and Magventure Inc. He is also on the scientific advisory board for Brainsway Inc. His work has been supported by the National Institutes of Mental Health (NIMH), the Canadian Institutes of Health Research (CIHR), Brain Canada, and the Temerty Family and Grant Family Foundations. DMB receives grant support from the Canadian Institutes of Health Research, the US National Institutes of Mental Health, Brain Canada, and the Temerty Family through the Centre for Addiction and Mental Health Foundation and the Campbell Research Institute. DMB received research support and in-kind equipment support for an investigator-initiated study from Brainsway. DMB was the site principal investigator for three sponsor-initiated studies for Brainsway. DMB received in-kind equipment support from Magventure for three investigator-initiated studies. DMB received medication supplies for an investigator-initiated trial from Indivior. DMB has participated in an advisory board meeting for Janssen and advisory board meeting for Welcony Inc. CL has served on the Scientific Advisory Board for Compass Pathways PLC, Delix Therapeutics, Brainify.AI, and Janssen Neuroscience and is listed as an inventor on Cornell University patent applications on neuroimaging biomarkers for depression that are pending or in preparation. LG and FMG report no biomedical financial interests or potential conflicts of interest.

References

1. Insel TR, Cuthbert BN (2015): Medicine. Brain disorders? Precisely. *Science* 348: 499–500.
2. Drysdale AT, Grosenick L, Downar J, Dunlop K, Mansouri F, Meng Y, *et al.* (2017): Resting-state connectivity biomarkers define neurophysiological subtypes of depression. *Nat Med* 23: 28–38.
3. American Psychiatric Association (2013): Diagnostic and Statistical Manual of Mental Disorders, 5th Edition (DSM-5). *Diagnostic and Statistical Manual of Mental Disorders 4th Edition TR.* https://doi.org/10.1176/appi.books.9780890425596.744053
4. Carroll BJ, Feinberg M, Greden JF, Tarika J, Albala AA, Haskett RF, *et al.* (1981): A specific laboratory test for the diagnosis of melancholia. Standardization, validation, and clinical utility. *Arch Gen Psychiatry* 38: 15–22.
5. Fried EI, Nesse RM (2015): Depression is not a consistent syndrome: An investigation of unique symptom patterns in the STAR*D study. *J Affect Disord* 172: 96–102.
6. Lewy AJ, Lefler BJ, Emens JS, Bauer VK (2006): The circadian basis of winter depression. *Proc Natl Acad Sci U S A* 103: 7414–9.
7. Lewy AJ, Sack RL, Miller LS, Hoban TM (1987): Antidepressant and circadian phase-shifting effects of light. *Science* 235: 352–4.
8. Wong ML, Kling MA, Munson PJ, Listwak S, Licinio J, Prolo P, *et al.* (2000): Pronounced and sustained central hypernoradrenergic function in major depression with melancholic features: relation to hypercortisolism and corticotropin-releasing hormone. *Proc Natl Acad Sci U S A* 97: 325–30.
9. Gold PW, Chrousos GP (2002): Organization of the stress system and its dysregulation in melancholic and atypical depression: high vs low CRH/NE states. *Mol Psychiatry* 7: 254–75.
10. Valerio MP, Szmulewicz AG, Martino DJ (2018): A quantitative review on outcome-to-antidepressants in melancholic unipolar depression. *Psychiatry Res* 265: 100–110.
11. Goodkind M, Eickhoff SB, Oathes DJ, Jiang Y, Chang A, Jones-Hagata LB, *et al.* (2015): Identification of a Common Neurobiological Substrate for Mental Illness. *JAMA Psychiatry* 5797: 305–315.
12. Oathes DJ, Patenaude B, Schatzberg AF, Etkin A (2015): Neurobiological signatures of anxiety and depression in resting-state functional magnetic resonance imaging. *Biol Psychiatry* 77: 385–93.
13. McTeague LM, Huemer J, Carreon DM, Jiang Y, Eickhoff SB, Etkin A (2017): Identification of Common Neural Circuit Disruptions in Cognitive Control Across Psychiatric Disorders. *Am J Psychiatry* 174: 676–685.
14. Greicius MD, Flores BH, Menon V, Glover GH, Solvason HB, Kenna H, *et al.* (2007): Resting-State Functional Connectivity in Major Depression: Abnormally Increased Contributions from Subgenual Cingulate Cortex and Thalamus. *Biol Psychiatry* 62: 429–437.
15. Sheline YI, Price JL, Yan Z, Mintun MA (2010): Resting-state functional MRI in depression unmasks increased connectivity between networks via the dorsal nexus. *Proc Natl Acad Sci U S A* 107: 11020–11025.
16. Kaiser RH, Andrews-Hanna JR, Wager TD, Pizzagalli DA (2015): Large-Scale Network Dysfunction in Major Depressive Disorder: A Meta-analysis of Resting-State Functional Connectivity. *JAMA Psychiatry* 72: 603–11.

17. Price RB, Gates K, Kraynak TE, Thase ME, Siegle GJ (2017): Data-Driven Subgroups in Depression Derived from Directed Functional Connectivity Paths at Rest. *Neuropsychopharmacology* 42: 2623–2632.
18. Pizzagalli DA (2014): Depression, stress, and anhedonia: toward a synthesis and integrated model. *Annu Rev Clin Psychol* 10: 393–423.
19. Price RB, Lane S, Gates K, Kraynak TE, Horner MS, Thase ME, Siegle GJ (2017): Parsing Heterogeneity in the Brain Connectivity of Depressed and Healthy Adults During Positive Mood. *Biol Psychiatry* 81: 347–357.
20. Clementz BA, Sweeney JA, Hamm JP, Ivleva EI, Ethridge LE, Pearlson GD, *et al.* (2016): Identification of distinct psychosis biotypes using brain-based biomarkers. *American Journal of Psychiatry* 173: 373–384.
21. Xia CH, Ma Z, Ciric R, Gu S, Betzel RF, Kaczkurkin AN, *et al.* (2018): Linked dimensions of psychopathology and connectivity in functional brain networks. *Nat Commun* 9: 3003.
22. Grisanzio KA, Goldstein-Piekarski AN, Wang MY, Rashed Ahmed AP, Samara Z, Williams LM (2018): Transdiagnostic Symptom Clusters and Associations With Brain, Behavior, and Daily Function in Mood, Anxiety, and Trauma Disorders. *JAMA Psychiatry* 75: 201–209.
23. Weigand A, Horn A, Caballero R, Cooke D, Stern AP, Taylor SF, *et al.* (2018): Prospective Validation That Subgenual Connectivity Predicts Antidepressant Efficacy of Transcranial Magnetic Stimulation Sites. *Biol Psychiatry* 84: 28–37.
24. Avissar M, Powell F, Ilieva I, Respino M, Gunning FM, Liston C, Dubin MJ (2017): Functional connectivity of the left DLPFC to striatum predicts treatment response of depression to TMS. *Brain Stimul* 10: 919–925.
25. Wu W, Zhang Y, Jiang J, Lucas M V, Fonzo GA, Rolle CE, *et al.* (2020): An electroencephalographic signature predicts antidepressant response in major depression. *Nat Biotechnol* 38: 439–447.
26. Kaiser RH, Chase HW, Phillips ML, Deckersbach T, Parsey R V, Fava M, *et al.* (2022): Dynamic Resting-State Network Biomarkers of Antidepressant Treatment Response. *Biol Psychiatry* 92: 533–542.
27. Padmanabhan JL, Cooke D, Joutsa J, Siddiqi SH, Ferguson M, Darby RR, *et al.* (2019): A Human Depression Circuit Derived From Focal Brain Lesions. *Biol Psychiatry* 86: 749–758.
28. Siddiqi SH, Taylor SF, Cooke D, Pascual-Leone A, George MS, Fox MD (2020): Distinct Symptom-Specific Treatment Targets for Circuit-Based Neuromodulation. *Am J Psychiatry* 177: 435–446.
29. Dunlop BW, Rajendra JK, Craighead WE, Kelley ME, McGrath CL, Choi KS, *et al.* (2017): Functional Connectivity of the Subcallosal Cingulate Cortex And Differential Outcomes to Treatment With Cognitive-Behavioral Therapy or Antidepressant Medication for Major Depressive Disorder. *Am J Psychiatry* 174: 533–545.
30. Fox MD, Liu H, Pascual-Leone A (2013): Identification of reproducible individualized targets for treatment of depression with TMS based on intrinsic connectivity. *Neuroimage* 66: 151–160.
31. Sharma A, Wolf DH, Ciric R, Kable JW, Moore TM, Vandekar SN, *et al.* (2017): Common Dimensional Reward Deficits Across Mood and Psychotic Disorders: A Connectome-Wide Association Study. *Am J Psychiatry* 174: 657–666.
32. Mihalik A, Ferreira FS, Rosa MJ, Moutoussis M, Ziegler G, Monteiro JM, *et al.* (2019): Brain-behaviour modes of covariation in healthy and clinically depressed young people. *Sci Rep* 9: 11536.

33. Feder S, Sundermann B, Wersching H, Teuber A, Kugel H, Teismann H, *et al.* (2017): Sample heterogeneity in unipolar depression as assessed by functional connectivity analyses is dominated by general disease effects. *J Affect Disord* 222: 79–87.
34. Grosenick L, Shi TC, Gunning FM, Dubin MJ, Downar J, Liston C (2019): Functional and Optogenetic Approaches to Discovering Stable Subtype-Specific Circuit Mechanisms in Depression. *Biol Psychiatry Cogn Neurosci Neuroimaging* 4: 554–566.
35. Goldstein-Piekarski AN, Ball TM, Samara Z, Staveland BR, Keller AS, Fleming SL, *et al.* (2021): Mapping Neural Circuit Biotypes to Symptoms and Behavioral Dimensions of Depression and Anxiety. *Biol Psychiatry*. https://doi.org/10.1016/j.biopsych.2021.06.024
36. Tokuda T, Yoshimoto J, Shimizu Y, Okada G, Takamura M, Okamoto Y, *et al.* (2018): Identification of depression subtypes and relevant brain regions using a data-driven approach. *Sci Rep* 8: 14082.
37. Buch AM, Vértes PE, Seidlitz J, Kim SH, Grosenick L, Liston C (2023): Molecular and network-level mechanisms explaining individual differences in autism spectrum disorder. *Nat Neurosci* 26: 650–663.
38. Wang H-T, Smallwood J, Mourao-Miranda J, Xia CH, Satterthwaite TD, Bassett DS, Bzdok D (2020): Finding the needle in a high-dimensional haystack: Canonical correlation analysis for neuroscientists. *Neuroimage* 216: 116745.
39. Dinga R, Schmaal L, Penninx BWJH, van Tol MJ, Veltman DJ, van Velzen L, *et al.* (2019): Evaluating the evidence for biotypes of depression: Methodological replication and extension of. *Neuroimage Clin* 22: 101796.
40. Marek S, Tervo-Clemmens B, Calabro FJ, Montez DF, Kay BP, Hatoum AS, *et al.* (2022): Reproducible brain-wide association studies require thousands of individuals. *Nature* 603: 654–660.
41. Spisak T, Bingel U, Wager TD (2023): Multivariate BWAS can be replicable with moderate sample sizes. *Nature* 615: E4–E7.
42. Zuo X-N, Kelly C, Adelstein JS, Klein DF, Castellanos FX, Milham MP (2010): Reliable intrinsic connectivity networks: test-retest evaluation using ICA and dual regression approach. *Neuroimage* 49: 2163–77.
43. Yan C-G, Cheung B, Kelly C, Colcombe S, Craddock RC, Di Martino A, *et al.* (2013): A comprehensive assessment of regional variation in the impact of head micromovements on functional connectomics. *Neuroimage* 76: 183–201.
44. Hamilton MC (1960): Hamilton Depression Rating Scale (HAM-D). *REDLOC* 23: 56–62.
45. Bagby RM, Ryder AG, Schuller DR, Marshall MB (2004): The Hamilton Depression Rating Scale: has the gold standard become a lead weight? *Am J Psychiatry* 161: 2163–77.
46. Rizvi SJ, Pizzagalli DA, Sproule BA, Kennedy SH (2016): Assessing anhedonia in depression: Potentials and pitfalls. *Neurosci Biobehav Rev* 65: 21–35.
47. Blumberger DM, Vila-Rodriguez F, Thorpe KE, Feffer K, Noda Y, Giacobbe P, *et al.* (2018): Effectiveness of theta burst versus high-frequency repetitive transcranial magnetic stimulation in patients with depression (THREE-D): a randomised non-inferiority trial. *Lancet* 391: 1683–1692.
48. Dunlop K, Sheen J, Schulze L, Fettes P, Mansouri F, Feffer K, *et al.* (2020): Dorsomedial prefrontal cortex repetitive transcranial magnetic stimulation for treatment-refractory major depressive disorder: A three-arm, blinded, randomized controlled trial. *Brain Stimul* 13: 337–340.
49. Beck AT, Steer RA, Brown GK (1996): Manual for the Beck depression inventory-II. *San Antonio, TX: Psychological Corporation* 1–82.

50. Rush AJ, Giles DE, Schlesser MA, Fulton CL, Weissenburger J, Burns C (1986): The Inventory for Depressive Symptomatology (IDS): preliminary findings. *Psychiatry Res* 18: 65–87.
51. Downar J, Geraci J, Salomons T v., Dunlop K, Wheeler S, McAndrews MP, *et al.* (2014): Anhedonia and Reward-Circuit Connectivity Distinguish Nonresponders from Responders to Dorsomedial Prefrontal Repetitive Transcranial Magnetic Stimulation in Major Depression. *Biol Psychiatry* 76: 176–185.
52. Cox RW (1996): AFNI: software for analysis and visualization of functional magnetic resonance neuroimages. *Comput Biomed Res* 29: 162–73.
53. Winkler AM, Renaud O, Smith SM, Nichols TE (2020): Permutation inference for canonical correlation analysis. *Neuroimage* 220: 117065.
54. Calinski T, Harabasz J (1974): A dendrite method for cluster analysis. *Commun Stat Theory Methods* 3: 1–27.
55. Lynch CJ, Power JD, Scult MA, Dubin M, Gunning FM, Liston C (2020): Rapid Precision Functional Mapping of Individuals Using Multi-Echo fMRI. *Cell Rep* 33: 108540.
56. Sheline YI, Barch DM, Price JL, Rundle MM, Vaishnavi SN, Snyder AZ, *et al.* (2009): The default mode network and self-referential processes in depression. *Proceedings of the National Academy of Sciences* 106: 1942–1947.
57. Wise T, Marwood L, Perkins AM, Herane-Vives A, Joules R, Lythgoe DJ, *et al.* (2017): Instability of default mode network connectivity in major depression: a two-sample confirmation study. *Transl Psychiatry* 7: e1105.
58. Renner F, Siep N, Arntz A, van de Ven V, Peeters FPML, Quaedflieg CWEM, Huibers MJH (2017): Negative mood-induction modulates default mode network resting-state functional connectivity in chronic depression. *J Affect Disord* 208: 590–596.
59. Aruldass AR, Kitzbichler MG, Morgan SE, Lim S, Lynall M-E, Turner L, *et al.* (2021): Dysconnectivity of a brain functional network was associated with blood inflammatory markers in depression. *Brain Behav Immun* 98: 299–309.
60. Miller OH, Bruns A, Ben Ammar I, Mueggler T, Hall BJ (2017): Synaptic Regulation of a Thalamocortical Circuit Controls Depression-Related Behavior. *Cell Rep* 20: 1867–1880.
61. Kerr CC, Kemp AH, Rennie CJ, Robinson PA (2011): Thalamocortical changes in major depression probed by deconvolution and physiology-based modeling. *Neuroimage* 54: 2672–82.
62. Zhang B, Lin P, Shi H, Öngür D, Auerbach RP, Wang X, *et al.* (2016): Mapping anhedonia-specific dysfunction in a transdiagnostic approach: an ALE meta-analysis. *Brain Imaging Behav* 10: 920–39.
63. Rzepa E, McCabe C (2016): Decreased anticipated pleasure correlates with increased salience network resting state functional connectivity in adolescents with depressive symptomatology. *J Psychiatr Res* 82: 40–7.
64. Germine LT, Garrido L, Bruce L, Hooker C (2011): Social anhedonia is associated with neural abnormalities during face emotion processing. *Neuroimage* 58: 935–45.
65. Wang L, Wang K, Liu J-H, Wang Y-P (2018): Altered Default Mode and Sensorimotor Network Connectivity With Striatal Subregions in Primary Insomnia: A Resting-State Multi-Band fMRI Study. *Front Neurosci* 12: 917.
66. Cheng Y, Xue T, Dong F, Hu Y, Zhou M, Li X, *et al.* (2021): Abnormal functional connectivity of the salience network in insomnia. *Brain Imaging Behav*. https://doi.org/10.1007/s11682-021-00567-9

67. Liu C-H, Liu C-Z, Zhu X-Q, Fang J-L, Lu S-L, Tang L-R, *et al.* (2018): Increased Posterior Insula-Sensorimotor Connectivity Is Associated with Cognitive Function in Healthy Participants with Sleep Complaints. *Front Hum Neurosci* 12: 35.
68. Liu C-H, Liu C-Z, Zhang J, Yuan Z, Tang L-R, Tie C-L, *et al.* (2016): Reduced spontaneous neuronal activity in the insular cortex and thalamus in healthy adults with insomnia symptoms. *Brain Res* 1648: 317–324.
69. Krepel N, Rush AJ, Iseger TA, Sack AT, Arns M (2020): Can psychological features predict antidepressant response to rTMS? A Discovery-Replication approach. *Psychol Med* 50: 264–272.
70. Rostami R, Kazemi R, Nitsche MA, Gholipour F, Salehinejad MA (2017): Clinical and demographic predictors of response to rTMS treatment in unipolar and bipolar depressive disorders. *Clin Neurophysiol* 128: 1961–1970.
71. Dunlop K, Victoria LW, Downar J, Gunning FM, Liston C (2021): Accelerated brain aging predicts impulsivity and symptom severity in depression. *Neuropsychopharmacology* 46: 911–919.
72. Talishinsky A, Downar J, Vértes PE, Seidlitz J, Dunlop K, Lynch CJ, *et al.* (2022): Regional gene expression signatures are associated with sex-specific functional connectivity changes in depression. *Nat Commun* 13: 5692.
73. Ichikawa N, Lisi G, Yahata N, Okada G, Takamura M, Hashimoto R-I, *et al.* (2020): Primary functional brain connections associated with melancholic major depressive disorder and modulation by antidepressants. *Sci Rep* 10: 3542.
74. Anand A, Li Y, Wang Y, Wu J, Gao S, Bukhari L, *et al.* (2005): Antidepressant effect on connectivity of the mood-regulating circuit: an FMRI study. *Neuropsychopharmacology* 30: 1334–44.
75. Scheidegger M, Walter M, Lehmann M, Metzger C, Grimm S, Boeker H, *et al.* (2012): Ketamine decreases resting state functional network connectivity in healthy subjects: implications for antidepressant drug action. *PLoS One* 7: e44799.
76. McCabe C, Mishor Z (2011): Antidepressant medications reduce subcortical-cortical resting-state functional connectivity in healthy volunteers. *Neuroimage* 57: 1317–23.
77. Posner J, Hellerstein DJ, Gat I, Mechling A, Klahr K, Wang Z, *et al.* (2013): Antidepressants normalize the default mode network in patients with dysthymia. *JAMA Psychiatry* 70: 373–82.
78. Wang L, Xia M, Li K, Zeng Y, Su Y, Dai W, *et al.* (2015): The effects of antidepressant treatment on resting-state functional brain networks in patients with major depressive disorder. *Hum Brain Mapp* 36: 768–78.
79. Dichter GS, Gibbs D, Smoski MJ (2015): A systematic review of relations between resting-state functional-MRI and treatment response in major depressive disorder. *J Affect Disord* 172: 8–17.
80. Korgaonkar MS, Goldstein-Piekarski AN, Fornito A, Williams LM (2020): Intrinsic connectomes are a predictive biomarker of remission in major depressive disorder. *Mol Psychiatry* 25: 1537–1549.
81. Berwian IM, Wenzel JG, Kuehn L, Schnuerer I, Kasper L, Veer IM, *et al.* (2020): The relationship between resting-state functional connectivity, antidepressant discontinuation and depression relapse. *Sci Rep* 10: 22346.
82. Buysse DJ, Reynolds CF, Monk TH, Berman SR, Kupfer DJ (1989): The Pittsburgh Sleep Quality Index: a new instrument for psychiatric practice and research. *Psychiatry Res* 28: 193–213.

Tables

Table 1: Demographic information for all MDD participants analyzed during regularized CCA.

	MDD
n	328
Female (%)	215 (65.6%)
Age (SD)	40.354 (12.047)
n HRSD (%)	328
HRSD (SD)	22.119 (4.784)
n BDI-II (%)	215 (65.5%)
BDI-II (SD)	37.58 (11.76)
n IDS (%)	113 (34.5%)
IDS (SD)	38.248 (8.486)

BDI-II: 21-item Beck Depression Inventory II(49); IDS: 28-item Inventory of Depressive Symptomatology(50); HRSD: 17-item Hamilton Rating Scale for Depression(44); MDD: Major Depressive Disorder; SD: Standard Deviation.

Figures

Figure 1: Assessing the performance of feature selection and regularized Canonical Correlation Analysis (CCA). (**A**) On average, most clinical items have numerous resting-state functional connectivity (RSFC) features that exceed chance. Violin plots visualizing the number of RSFC features correlated with each clinical item at $p < 0.05$ using bootstrapping (1,000 replicates). Points indicate percentage of all 33,153 RSFC features that exceeded chance at $p < 0.05$, whole brain. The red bar indicates the chance number of clinical loadings, which has been standardized such that chance = 0. The first 16 items represent the Hamilton Rating Scale for Depression items, while the last 5 represent composite score from homologous items of the Beck Depression Inventory II and Inventory of Depressive Symptomatology. (**B**) Grid search hyperparameter optimization suggests that the optimal hyperparameters are: 300 RSFC features per clinical item, RSFC regularization λ (y-axes) = 100, and clinical regularization λ (x-axes) = 0.1. Heatmaps represent the average canonical correlation for canonical variate 1 when projected to data held-out during training within the inner fold (2/3 train, 1/3 test; 2,000 replicates). (**C**) The first three canonical variates significantly replicate in held-out data. Black kernel density estimations represent the histogram of permuted data (1,000 replicates), whereas the red line indicates the average test canonical correlation across 1,000 unshuffled replicates. For replicability in test data, the x-axis represents the canonical correlation of each canonical variate (CV) in test data at the optimal combination of hyperparameters identified in (B); greater canonical correlations in unshuffled data indicates a better fit of the regularized CCA model to test data. Corrected *p*-values (in red) were obtained using the null distribution. (**D**) The first three canonical variates have significantly stable clinical loadings. The x-axes represent the absolute correlation of clinical loadings; a higher score indicates greater agreement in clinical loadings across all training replicates. Black kernel density estimations represent the histogram of permuted training data (1,000 replicates), whereas the red line indicates the average training clinical loading correlation across 1,000 unshuffled replicates for each CV. Corrected *p*-values (in red) were obtained using the null distribution. (**E-G**) Results of the regularized CCA model, using the optimal combination of hyperparameters identified in Figure 1B, and using the entire sample (n = 328). Each figure section represents the following two images for each canonical variate (CV), from left to right: (I) A scatterplot visualizing the canonical correlation, with rho values displayed at the top. (II) significant clinical loadings, Bonferroni-corrected for the number of clinical items ($q = 0.002$). Black cells indicate that the clinical item was not statistically significant after correcting for multiple comparisons and heatmap values indicate the Pearson correlation coefficient of the clinical item severity and the CV scores in the clinical dimension. Higher values indicate a greater positive correlation between symptom severity and canonical variate score.

Figure 2: Regularized Canonical Correlation Analysis (CCA) yields three canonical variates of distinct symptomatology and resting-state functional connectivity (RSFC). **(A-C**) Results of the regularized CCA model, using the optimal combination of hyperparameters identified in Figure 1B, and using the entire sample (n = 328). Each figure section represents the following two images for each canonical variate (CV), from left to right: (I) The top 25 regions of interest associated with each canonical variate, identified as the sum of coefficients of determination for surviving features at FDR-$p < 0.05$, whole-brain. Only the right hemisphere is visualized, and regions of interest are color-coded by network. (II) Network-binned RSFC loadings for the top 25 regions of interest. Top regions of interest from the same network and region were binned to identify the mean RSFC loading (Pearson correlation coefficient, FDR-corrected) for intrinsic brain networks. Black cells indicate that no RSFC features remained after correcting for multiple comparisons. Canonical variate 1 was associated with depressed mood and general somatic symptoms, and more severe severity on these symptoms was associated with increased default mode/subcortical RSFC, and decreased default mode-cingulo-opercular RSFC. Canonical variate 2 was associated with anhedonia. Greater cingulo-opercular, attentional, and visual RSFC was associated with greater anhedonia. Canonical variate 3 was associated with insomnia and sensorimotor RSFC; higher sensorimotor RSFC was associated with less mild/absent insomnia, but more severe mood and irritability. (**D**) Venn diagram depicting the degree of overlap between the three canonical variates' significant RSFC features. Only 4 RSFC features were significantly associated with individual symptom differences for all three canonical variates. (**E**) Venn diagram depicting the degree of overlap between the three canonical variates' significant RSFC features and atypical RSFC in all MDD participants relative to nondepressed controls. Abbreviations: aCOTC: prefrontal/insular nodes of the cingulo-opercular network; aDAN: prefrontal nodes of the dorsal attention network; aDMN: prefrontal nodes of the default mode network; aFPN: prefrontal nodes of the fronto-parietal network; aVAN: prefrontal nodes of the ventral attention network; BG: basal ganglia; C: composite clinical item; CV: canonical variate; dACC/SMA: dorsal anterior cingulate cortex and supplementary motor area; DLPFC: dorsolateral prefrontal cortex; H: Hamilton clinical item; HC: healthy controls; Ins.: Insula; MDD: major depressive disorder; OFC: orbitofrontal cortex; pCOTC: parieto-temporal nodes of the cingulo-opercular network; PCC: posterior cingulate cortex; pDAN: parieto-temporal nodes of the dorsal attention network; pDMN: parieto-temporal nodes of the default mode network; pFPN: parieto-temporal nodes of the fronto-parietal network; Phys.: physiological; pIns: posterior insula; Psych.: psychological; pVAN: parieto-temporal nodes of the ventral attention network; ROI: region of interest; RSFC: resting-state functional connectivity; Thal.: thalamus; TPJ: temporo-parietal junction; V1: primary visual cortex; V5: middle temporal visual area; Vis.: visual; VMPFC: ventromedial prefrontal cortex.

Figure 3: Hierarchical clustering yields four robust and stable subtypes with distinct symptom severity. (**A**) Dendrogram visualizing the optimal $k = 4$ solution using the first two canonical variates. Heatmap values indicate participants' canonical variate scores in the RSFC dimension (arbitrary units). (**B**) Scatterplot visualizing the four clusters by canonical variate score. The x- and y-axes represent the canonical variate scores 1 and two, respectively. (**C**) Calinski-Harabasz criteria values evaluating 2-10 cluster solutions when suing the first two canonical variates. Higher values indicate better performance in terms of the within- and between-cluster variance. The red asterisk indicates candidate hierarchical clustering solutions, which represents a peak in the Calinski-Harabasz criterion at $k = 4$. (**D**) Permutation testing indicates that the $k = 4$ clustering solution using the first two variates performs significantly better than that expected by chance. The violin plot represents the distribution of Calinski-Harabasz Criterion values for permuted training data; the red point indicates the criterion value for the unshuffled cluster solution. (**E**) Adjusted mutual information assessing the concordance of cluster membership in two-thirds subsamples of data relative to membership obtained using the entire sample (error bars = standard error of the mean). The elbow is at $k = 3$ clusters using the first two canonical variates. (**F**) Permutation testing the candidate optimal solution, $k = 4$ clusters, using the first two canonical variates. Cluster membership in two-thirds subsamples relative to the membership obtained using the complete sample for this potential clustering solution performed significantly greater than chance. The kernel density estimation represents the distribution of adjusted mutual information values in shuffled data, while the red line indicates the mean adjusted mutual information of the true sample. (**E-G**) Boxplots visualizing dimension scores for canonical variates 1 (E), 2 (F), and 3 (G). Asterisks indicate significant differences at FDR-$p < 0.05$. There were robust differences by subtype for the first two canonical variates. (**H**) Mean clinical severity by subtype for the Hamilton Rating Scale for Depression and composite scores; error bars represent the standard error of the mean. Asterisks represent subtype-specific significant differences (FDR-$p < 0.05$) relative to the severity of the entire sample. Asterisks indicate significant differences at FDR-$p < 0.05$. Abbreviations: C: composite score; CV: canonical variate; H: Hamilton Rating Scale for Depression item.

Figure 4: Biologically-based subtypes exhibit distinct abnormal resting-state functional connectivity (RSFC) and responsivity to repetitive transcranial magnetic stimulation (rTMS). (**A**) The top 25 most distinct regions of interest in terms of subtype-specific atypical RSFC, identified using a Kruskal-Wallis test. (**B-E**) Network-binned RSFC loadings for the top 25 most divergent regions of interest across all four subtypes. ROIs from the same network and region were binned to identify the mean RSFC loading (*z*-score from a Wilcoxon rank sum test between subtypes and controls, FDR-corrected) for intrinsic brain networks. Black cells indicate that no RSFC features remained after correcting for multiple comparisons. Higher values indicate subtype hyperconnectivity relative to nondepressed controls. (**F**) Network-binned RSFC loadings representing atypical RSFC in all MDD participants relative to healthy controls, using the top 25 ROIs visualized in (B). (**G**) Venn diagram depicting the degree of overlap between significantly abnormal RSFC features present in the MDD *versus* healthy controls contrast, and RSFC features that were atypical in one or more subtypes. (**H**) Venn diagram depicted the degree of overlap between RSFC features that were significantly atypical in one or more subtypes and significantly associated with symptom dimensions (canonical variate loadings). (**I**) Differences in antidepressant response and remission to active rTMS (dorsolateral or dorsomedial rTMS, both 10 Hz and intermittent theta burst). Response was defined as ≥50% improvement from baseline to end of treatment on the Hamilton Rating Scale for Depression, and remission was defined as <9 on the same scale at the end of treatment. (**J-M**) Significant main effects and interactions from a binomial logistic regression predicting remission status. There was a significant main effect of canonical variate 2 score (**J-K**), such that a higher dimension score (lower anhedonia severity) resulted in a greater probability of remission, irrespective of stimulation site or treatment parameters. Furthermore, there was a significant interaction effect with canonical variate 1 (mood/somatic symptoms; **L-M**), such that dimension scores were differentially associated with 10 Hz and TBS remission. Abbreviations: aCOTC: anterior nodes of the cingulo-opercular task-control network; anterior nodes of the dorsal attention network; aDMN: anterior nodes of the default mode network; aFPN: anterior nodes of the fronto-parietal network; aVAN: anterior nodes of the ventral attention network; CV: canonical variate; DLPFC: dorsolateral prefrontal cortex; dVis: higher order visual, dorsal stream; IPS: intraparietal sulcus; NR: Non-Remitter; OFC: orbitofrontal cortex; Parahipp.: parahippocampal gyrus; pCOTC: posterior nodes of the cingulo-opercular task-control network; pDAN: posterior nodes of the dorsal attention network; pDMN: posterior nodes of the default mode network; pFPN: posterior nodes of the fronto-parietal network; pVAN: posterior nodes of the ventral attention network; R: Remitter; rTMS: repetitive transcranial magnetic stimulation; sgACC: subgenual cingulate cortexStr.: Striatum; TBS: theta burst stimulation; Thal.: thalamus; vVis: higher order visual, ventral stream.